

Improvement to Water Speciation and FeCO₃ Precipitation Kinetics in CO₂ Environments: Updates in NaCl Concentrated Solutions

Zheng Ma, Xin Gao, Bruce Brown, Srdjan Nestic, and Marc Singer*



Cite This: *Ind. Eng. Chem. Res.* 2021, 60, 17026–17035



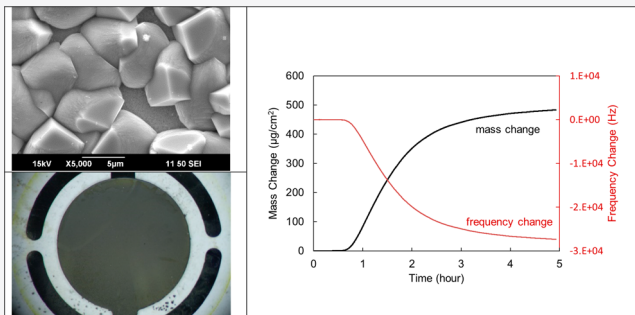
Read Online

ACCESS |

Metrics & More

Article Recommendations

ABSTRACT: In the oil and gas industry, the dissolution rate of metal-based materials exposed to an aqueous phase is often controlled by the presence of surface layers such as corrosion products. Knowing the characteristics and rate of formation of these surface layers can help assess the level of protection against corrosion they provide and can permit the development of a successful asset integrity program. The appropriate determination of species concentration is a key aspect of accurately predicting the precipitation rate of corrosion products, more specifically of FeCO₃, which is the main product of corrosion of steel in CO₂-containing environments. While aqueous speciation in low-salinity brine is well-established, the effects of high NaCl contents (NaCl ≥ 3 wt %) on water chemistry and FeCO₃ precipitation are less defined. In this work, two fundamental aspects of H₂O/Fe/CO₂ system speciation in high salinity brine are discussed: the consumption of Fe²⁺ due to the formation of ferrous chloride (FeCl⁺) complex and the dependence of K_{ca} , the first dissociation constant of H₂CO₃, on ionic strength. This leads to a comprehensive revision of the models used to calculate the solubility product of iron carbonate (FeCO₃), $K_{sp,FeCO_3}$. In parallel, the kinetics of FeCO₃ precipitation are experimentally investigated using an electrochemical quartz crystal microbalance (EQCM) in concentrated NaCl solutions at varied temperatures (50–80 °C). This led to the development of a new kinetics model for FeCO₃ precipitation that now considers the nonideality of the solutions.

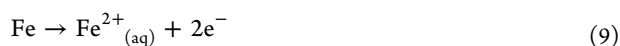


INTRODUCTION

Corrosion prevention and control represent an important issue of study in the oil and gas industry, as internal corrosion of a pipeline is encountered during daily operation. The aqueous CO₂ corrosion of carbon steel includes a complex system of interrelated processes that contains homogeneous aqueous CO₂ chemical reactions and electrochemical reactions at the surface of carbon steel. The heterogeneous precipitation of iron carbonate (FeCO₃), the most common corrosion product in aqueous CO₂ corrosion of mild steel, may be triggered at the surface of carbon steel depending on the operating conditions.¹

CO₂ gas is not corrosive by itself. However, as it dissolves in an aqueous solution, as shown in reaction 1, it will lead to the formation of a weak acid. The chemistry of an aqueous solution containing dissolved CO_{2(aq)} involves the hydration of CO_{2(aq)} to form carbonic acid (reaction 3), H₂CO₃ (a weak acid), followed by two partial dissociation steps (reactions 5 and 7). These chemical reactions, as well as the expressions of the corresponding equilibrium constants, are listed in Table 1.

Iron is then electrochemically dissolved at the anodic site to release ferrous ions when corrosion occurs:



Simultaneously, hydrogen ion reduction takes place at the cathodic site:²



FeCO₃ precipitates from solution via the following reaction:



when the concentration product of Fe²⁺_(aq) and CO₃²⁻_(aq) exceeds the solubility product, $K_{sp,FeCO_3}$, as defined by eq 12, where $c_{\text{Fe}^{2+}}$ and $c_{\text{CO}_3^{2-}}$ (mol·L⁻¹) are the equilibrium aqueous concentration of Fe²⁺ and CO₃²⁻, and $K_{sp,FeCO_3}$ (mol²·L⁻²) is a function that depends on both temperature (T_K in Kelvin) and ionic strength (I in mol·L⁻¹):

Received: July 27, 2021

Revised: September 28, 2021

Accepted: September 29, 2021

Published: November 9, 2021

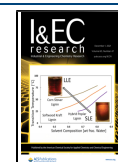


Table 1. Chemical Reactions in an Aqueous CO₂ Solution and Corresponding Equilibrium Expressions

name	chemical reaction	equilibrium expression
CO ₂ dissolution	CO _{2(g)} ⇌ CO _{2(aq)} (1)	$K_{\text{sol,CO}_2} = \frac{c_{\text{CO}_2}}{p_{\text{CO}_2}}$ (2)
CO ₂ hydration	CO _{2(aq)} + H ₂ O(l) ⇌ H ₂ CO _{3(aq)} (3)	$K_{\text{hyd}} = \frac{c_{\text{H}_2\text{CO}_3}}{c_{\text{CO}_2}}$ (4)
carbonic acid dissociation	H ₂ CO _{3(aq)} ⇌ H ⁺ _(aq) + HCO ₃ ⁻ _(aq) (5)	$K_{\text{ca}} = \frac{c_{\text{HCO}_3^-} \times c_{\text{H}^+}}{c_{\text{H}_2\text{CO}_3}}$ (6)
bicarbonate ion dissociation	HCO ₃ ⁻ _(aq) ⇌ H ⁺ _(aq) + CO ₃ ⁻² _(aq) (7)	$K_{\text{bi}} = \frac{c_{\text{CO}_3^{-2}} \times c_{\text{H}^+}}{c_{\text{HCO}_3^-}}$ (8)

$$K_{\text{sp,FeCO}_3} = c_{\text{Fe}^{2+}} \times c_{\text{CO}_3^{2-}} \quad (12)$$

where the ionic strength, a parameter that is used to represent the nonideal behavior in water chemistry,^{3–6} can be calculated from the concentration c_j and charge z_j of different species in the solution:

$$I = \frac{1}{2} \sum_j c_j z_j^2 \quad (13)$$

Oddo and Tomson created a set of empirical equations⁷ to determine some of the equilibrium constants mentioned above based on ionic strength and partial pressure of CO₂:

$$K_{\text{sol,CO}_2} = \frac{14.5}{1.00258} \times 10^{-(2.27+5.65 \times 10^{-3} T_f - 8.06 \times 10^{-6} T_f^2 + 0.075 I)} \quad (14)$$

$$K_{\text{ca}} = 387.6 \times 10^{-(6.41 - 1.594 \times 10^{-3} T_f + 8.52 \times 10^{-6} T_f^2 - 3.07 \times 10^{-5} p_{\text{CO}_2} - 0.4772 I^{1/2} + 0.11807 I)} \quad (15)$$

$$K_{\text{bi}} = 10^{-(10.61 - 4.97 \times 10^{-3} T_f + 1.331 \times 10^{-5} T_f^2 - 2.624 \times 10^{-5} p_{\text{CO}_2} - 1.166 I^{1/2} + 0.3466 I I)} \quad (16)$$

where T_f is temperature in Fahrenheit and p_{CO_2} is partial pressure of CO₂ in psi. The value of K_{hyd} was determined to be 2.58×10^{-3} at 25 °C and 2.31×10^{-3} at 300 °C by Palmer and Eldik.⁸

The Oddo–Tomson model has been widely circulated in CO₂ related water chemistry calculation.^{1,9–11} However, when comparing the predicted pH using Oddo–Tomson model with experimental data at three different temperatures (80, 50, and 30 °C), Gao¹² noticed the predictions are close to the measurements only when the NaCl concentration in solution is lower than 5 wt % ($I < 0.9 \text{ mol} \cdot \text{L}^{-1}$) and deviate more and more from the measurements as the NaCl concentration is increased. All three equilibrium constants in the Oddo–Tomson model are ionic-strength-dependent and affect the accuracy of pH prediction. Among these three constants, it was shown¹² that the concentration of dissolved carbon dioxide, c_{CO_2} , calculated using $K_{\text{sol,CO}_2}$, agrees well with measurements.¹³ K_{bi} is significantly smaller than K_{ca} (by about 5 orders of magnitude) under the tested conditions; thus, the proton production through reaction 7 is negligible as compared to that by reaction 5. On the basis of these observations, it can be concluded that the inaccuracy behind the expression of K_{ca} plays a key role in explaining the deviation and the eq 15 should be revised.

Efforts have been made to develop mathematical correlations between $K_{\text{sp,FeCO}_3}$ versus temperature^{14–19} and $K_{\text{sp,FeCO}_3}$ versus I .²⁰ After comparing the predictions with measurements across different studies, a $K_{\text{sp,FeCO}_3}$ model, that includes the effects of temperature and ionic strength simultaneously, was developed by Sun and Nescic²¹ by numerically combining a temperature-dependent $K_{\text{sp,FeCO}_3}$ model proposed by Greenberg and Tomson¹⁴ together with an ionic-strength-dependent $K_{\text{sp,FeCO}_3}$ model proposed by Silva et al.²⁰

$$\log K_{\text{sp,FeCO}_3} = -59.3498 - 0.041377 T_K - \frac{2.1963}{T_K} + 24.5724 \log T_K + 2.518 I^{0.5} - 0.657 I \quad (17)$$

This equation has been used in corrosion models^{9,22} as well as FeCO₃ precipitation kinetics models.^{23,24} However, in their recent work, Gao¹² challenged the above-mentioned expression of $K_{\text{sp,FeCO}_3}$ and showed that the predicted $K_{\text{sp,FeCO}_3}$ starts to deviate from measurements in a 5 wt % NaCl brine, and the deviation keeps increasing with the increase of the NaCl concentration in solutions. To solve this, Gao proposed some modifications to the two ionic-strength-dependent terms in eq 17 to better fit the measurements. Unfortunately, the possibility of forming ferrous chloride (FeCl⁺),^{25,26} a complex that tends to form in chloride-containing solutions, was not considered in their work. This leaves the validity of the $K_{\text{sp,FeCO}_3}$ equations contentious, as the formation of FeCl⁺ could significantly decrease the actual amount of freely available ferrous ions in solutions.

The formation of FeCO₃ on a steel surface is believed to influence the corrosion process,^{27–29} and several models have been developed to predict FeCO₃ precipitation kinetics based on experimental measurements.^{14,25,24,30,31} Sun was the first to propose a model (S&N model) based on measuring the mass of FeCO₃ precipitated directly on a steel sample.²³ Other models developed before the S&N model determined the precipitated FeCO₃ mass indirectly via tracking the change of Fe²⁺ concentration in bulk solution.^{14,30,31} Because of this difference in experimental methodology, it has been argued that the S&N model provides more accurate predictions.²³ A later model proposed by Ma et al.²⁴ confirmed that the driving force for the precipitation process is a function of ($S_{\text{FeCO}_3} - 1$) and that the precipitation rate (PR_{FeCO_3}) could be calculated following the equation suggested by the S&N model:

$$PR_{\text{FeCO}_3} = k_{r,\text{FeCO}_3} e^{-\Delta^* G_{\text{FeCO}_3}/RT} K_{\text{sp,FeCO}_3} (S_{\text{FeCO}_3} - 1) \quad (18)$$

where $k_{r,FeCO_3}$ in $m^4 \cdot mol^{-1} \cdot s^{-1}$ is the kinetic constant, $\Delta^*G_{FeCO_3}$ in $J \cdot mol^{-1}$ is the activation energy of $FeCO_3$ precipitation, and the saturation level of $FeCO_3$, S_{FeCO_3} , is defined as

$$S_{FeCO_3} = \frac{c_{Fe^{2+},free} \times c_{CO_3^{2-}}}{K_{sp,FeCO_3}} \quad (19)$$

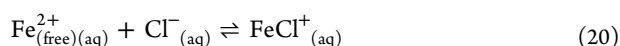
$c_{Fe^{2+},free}$ represents the concentration of freely available ferrous ions in solutions.

By using electrochemical quartz crystal microbalance (EQCM), Ma et al.²⁴ were able to monitor the real-time mass change of precipitated $FeCO_3$ on sample surface. This technique largely enhanced the accuracy of the measurements, as the S&N model was based on the measurements of the time-averaged mass change of precipitated $FeCO_3$. However, the updated values of $k_{r,FeCO_3}$ ($3.32 \times 10^7 m^4 \cdot mol^{-1} \cdot s^{-1}$) and $\Delta^*G_{FeCO_3}$ ($73\,739 J \cdot mol^{-1}$) obtained in Ma et al.'s work cannot yet be directly applied in most of the nonideal solutions. These two parameters were calibrated in only 1 wt % NaCl solution, and they were calibrated based on incorrect S_{FeCO_3} values. The expressions used to calculate $c_{CO_3^{2-}}$ and $K_{sp,FeCO_3}$ have been shown to be inaccurate in NaCl concentrated solutions; instead of $c_{Fe^{2+},total}$ total $c_{Fe^{2+}}$ (including both $FeCl^+$ and freely available Fe^{2+}) was mistakenly used during the calculations. These issues are nevertheless only significant at high NaCl contents.

In this paper, the effect of salinity on the consumption of Fe^{2+} is evaluated as a function of temperature and NaCl concentration (in terms of ionic strength), and updates are proposed to the equations used to determine K_{ca} , the first dissociation constant of H_2CO_3 , and the solubility product of $FeCO_3$, $K_{sp,FeCO_3}$. Beyond that, the precipitation kinetics of $FeCO_3$ are investigated using EQCM in solutions with varied NaCl concentrations to elucidate the effect of solution salinity on $FeCO_3$ precipitation kinetics.

■ IMPROVEMENT TO WATER SPECIATION IN CO_2 ENVIRONMENTS

Freely Available Fe^{2+} in NaCl Solutions. As introduced above, the actual amount of Fe^{2+} in solution that is freely available for $FeCO_3$ precipitation is dependent on the formation of $FeCl^+$ complex in NaCl aqueous solutions.²⁵ The formation reaction for $FeCl^+$ is considered as follows:



Its corresponding equilibrium constant expression, K_1 , is thus defined as

$$K_1 = \frac{a_{FeCl^+}}{a_{Fe^{2+}} \times a_{Cl^-}} \quad (21)$$

where a_j , the activity of species j , is the product of molality m_j in $mol/kg(H_2O)$ and activity coefficient γ_j ; K_1 is dependent on temperature as follows:²⁵

$$\log K_1 = -7.1783 + \frac{911.13}{T_K} + 0.013407T_K \quad (22)$$

Meanwhile, assuming that no other Fe^{2+} complexes form, the mass balance on Fe^{2+} (eq 23), can be used to express the total ferrous species molality in solution, $m_{Fe^{2+},total}$ as a function of the molality of $FeCl^+$, m_{FeCl^+} , and free Fe^{2+} , $m_{Fe^{2+},free}$:

$$m_{FeCl^+} + m_{Fe^{2+},free} = m_{Fe^{2+},total} \quad (23)$$

The molality ratio between the free Fe^{2+} and total Fe^{2+} , $R_{Fe^{2+}}$, can thus be calculated if eqs 21 and 23 are combined:

$$R_{Fe^{2+}} = \frac{m_{Fe^{2+},free}}{m_{Fe^{2+},total}} = \frac{\gamma_{FeCl^+}}{K_1 \cdot \gamma_{Fe^{2+}} \cdot m_{Cl^-} \cdot \gamma_{Cl^-} + \gamma_{FeCl^+}} \quad (24)$$

This clearly shows that $R_{Fe^{2+}}$ is dependent on the nonideality of the given solution,^{25,26} as indicated by the presence of activity coefficients, which cannot be assumed to be unity in highly concentrated solutions.

On the basis of eqs 22 and 24, the dependency of $R_{Fe^{2+}}$ on temperature can be mathematically examined. By considering solutions containing 100 ppm (wt) total Fe^{2+} and pH 6.6 as an example (a condition that was normally used for $FeCO_3$ precipitation experiment as will be covered in a later section), $R_{Fe^{2+}}$ has only a marginal dependence on temperature, both with 1 and 25 wt % NaCl solutions. Only about 4% more $FeCl^+$ is formed when the temperature is raised from 10 to 90 °C in solution with 1 wt % NaCl, and there is almost no change in $R_{Fe^{2+}}$ for 25 wt % NaCl over the same temperature range.

The effect of NaCl concentration on $R_{Fe^{2+}}$ is much stronger as shown in Figure 1 (90 °C, 100 ppm (wt) total Fe^{2+} and pH

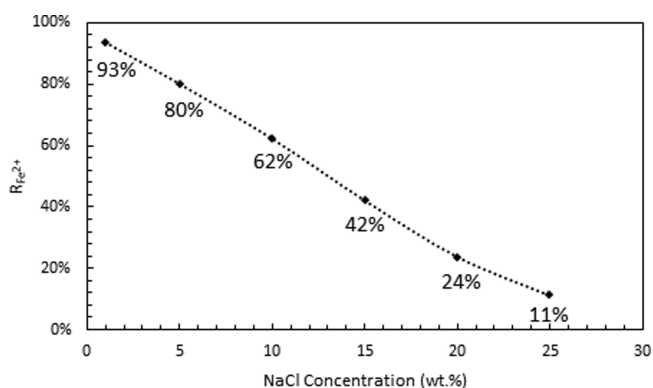


Figure 1. $R_{Fe^{2+}}$ dependence on NaCl concentration with 100 ppm (wt) total Fe^{2+} and pH 6.6.

6.6). At 90 °C, $R_{Fe^{2+}}$ is 93% with 1 wt % NaCl, suggesting that 7% of Fe^{2+} is already converted to $FeCl^+$. However, $R_{Fe^{2+}}$ decreases to 62% when the solution contains 10 wt % NaCl, meaning that close to half of the total Fe^{2+} ions is no longer available as free Fe^{2+} . With 25 wt % NaCl, about 90% of the total Fe^{2+} ions are in the form of $FeCl^+$ complexes. This leaves only 10% of the total Fe^{2+} ions free and available to possibly precipitate into $FeCO_3$. On the basis of this observation, it can be concluded that any calculation ignoring the formation of $FeCl^+$ could lead to an overestimation of the free Fe^{2+} concentration and consequently of S_{FeCO_3} , especially with high NaCl content.

Many research works bypass the calculation complexity of nonideal models (i.e., use of activity coefficients in eq 24) by considering the effect of ionic strength, I . This parameter reflects the solution nonideality^{7,12,20,23,27} and is much easier to access and implement; however, there is a cost in terms of model accuracy and expandability. Since many models still use the "ionic strength" approach (instead of the "activity" approach as in eqs 21 and 24), the development of a correlation identifying the dependence of $R_{Fe^{2+}}$ on ionic

strength would be quite valuable as it would greatly simplify the calculation process. To fulfill this purpose, the equilibrium constant for reaction 20 is redefined in the form of concentration (mol/L) instead of activity:

$$K_2 = \frac{c_{\text{FeCl}^+}}{c_{\text{Fe}^{2+}}c_{\text{Cl}^-}} \quad (25)$$

Since the total concentration of Fe^{2+} , $c_{\text{Fe}^{2+}_{\text{total}}}$, is conserved in solution, K_2 can also be calculated via the following equation:

$$K_2 = \frac{c_{\text{Fe}^{2+}_{\text{total}}} - c_{\text{Fe}^{2+}}}{c_{\text{Fe}^{2+}}c_{\text{Cl}^-}} \quad (26)$$

It is now assumed that K_2 , calculated via concentration, should follow the same dependency with temperature as for K_1 . Furthermore, the nonideality of the solution is addressed by including an ionic strength dependency in the expression of K_2 . Consequently, K_2 can be expressed in terms representing its dependency on temperature and ionic strength:

$$\log K_2 = f(I)_{K_2} + \frac{911.13}{T_K} - 0.013407T_K \quad (27)$$

This leads to eq 28 after putting the temperature terms together with $\log K_2$ and moving the ionic-strength-dependent term $f(I)_{K_2}$ to the left-hand side of the equation:

$$f(I)_{K_2} = \log K_2 - \frac{911.13}{T_K} + 0.013407T_K \quad (28)$$

In order to derive K_2 , an in-house solver (WELLCORP),³⁴ based on the Pitzer activity model, was employed to calculate molalities and activity coefficients of species in solutions with 1, 5, 10, 15, and 25 wt % NaCl at varied temperatures from 10 to 90 °C at a 10 °C interval. The corresponding concentrations in molality (mol/kg) are converted to molarity (mol/L) when the solution density for water (ρ_W in g/cm³, eq 29) and for brine (ρ_B in g/cm³, eq 30)³⁵ and solution volume in L (eq 31) are known:

$$\begin{aligned} \rho_W = & 1 + 1 \times 10^6(-80T_c - 3.3T_c^2 + 0.00175T_c^3 + 489P \\ & - 2T_cP + 0.016T_c^2P - 1.3 \times 10^{-5}T_c^3P - 0.333P^2 \\ & - 0.002T_cP) \end{aligned} \quad (29)$$

$$\begin{aligned} \rho_B = & \rho_W + c_{\text{NaCl}}\{0.668 + 0.44c_{\text{NaCl}} \\ & + 1 \times 10^{-6}[300P - 2400Pc_{\text{NaCl}} + T_c(80 + 3T_c \\ & - 3300c_{\text{NaCl}} - 13P + 47Pc_{\text{NaCl}})]\} \end{aligned} \quad (30)$$

$$\text{Vol. of Brine} = \frac{\text{total mass of NaCl and H}_2\text{O}}{\rho_B} \quad (31)$$

where T_c is the temperature in Celsius, P is the total pressure in Mpa, and c_{NaCl} is the weight fraction of NaCl.

$f(I)_{K_2}$ is plotted against $I^{0.5}$ (where the black dots are the calculated $f(I)_{K_2}$ over different temperatures and salt concentrations) in Figure 2. A dependency with $I^{0.5}$, rather than I , results in a better fit. The complete expression of K_2 can then be derived using a non-linear least-squares fitting method, and its final equation is written as eq 32:

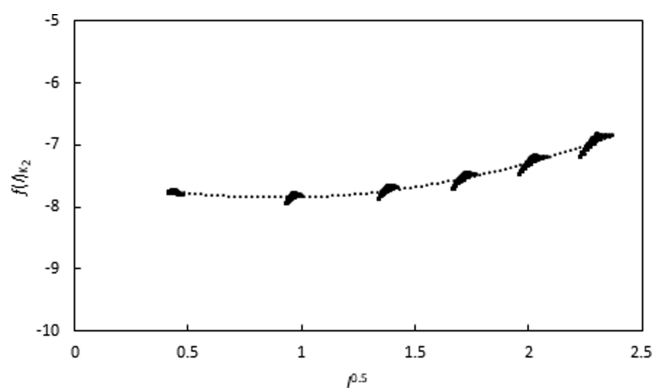


Figure 2. Fitting line for $f(I)_{K_2}$ vs $I^{0.5}$ for temperature between 10 to 90 °C.

$$\begin{aligned} \log K_2 = & -7.4798 + 0.013407T_K + \frac{911.13}{T_K} + 0.4561I \\ & - 0.816I^{0.5} \end{aligned} \quad (32)$$

Revision of K_{ca} . The expression of K_{ca} originally proposed by Oddo and Tomson¹² refers to concentrations (instead of activities) and already includes a dependence on $I^{0.5}$, as shown in eq 15.⁷ The expression agrees well with experimental measurements in solutions containing relatively low NaCl concentration (≤ 5 wt %) over a wide range of temperatures. However, a deviation appears in more concentrated solutions, which signals a need to adjust the terms initially proposed to cover the effect of ionic strength.

Equation 15 is rewritten to isolate the ionic strength and the temperature-pressure-dependent terms, as shown in eq 33. The ionic strength term (denoted as $f(I)_{K_{ca}}$) is used to quantify the updated dependence on ionic strength by plotting the values calculated at different temperatures against I . An expression for $f(I)$ can then be obtained using a nonlinear least-squares fitting method.

$$\begin{aligned} f(I)_{K_{ca}} = & \log 387.6 - \log K_{ca} + 1.594 \times 10^{-3}T_f \\ & - 8.52 \times 10^{-6}T_f^2 + 3.07 \times 10^{-5}p_{\text{CO}_2} \end{aligned} \quad (33)$$

Experimental values for K_{ca} were determined by collecting measured pH over different temperatures (5–80 °C) in solutions containing dissolved CO_2 (0.53–0.99 bar) and with various salt concentrations (0.1–25 wt %) from the literature.^{12,36,37} Equation 33 is plotted against $I^{0.5}$ as dots in Figure 3, where the dotted line is the best fit obtained over the entire range of temperature selected. As can be seen from the figure, rather than the quadratic correlation with $I^{0.5}$ as suggested by eq 15,⁷ as well as proposed by the expressions of Oddo and Tomson⁷ and Gao,¹² the best fit involves a linear dependency with $I^{0.5}$. This agrees with experimental results measured by Lyman³⁸ and Mehrbach et al.³⁹ The final equation of K_{ca} is written as eq 34:

$$\begin{aligned} K_{ca} = & 387.6 \\ & \times 10^{-(6.6216 - 1.594 \times 10^{-3}T_f + 8.52 \times 10^{-6}T_f^2 - 3.07 \times 10^{-5}p_{\text{CO}_2} - 0.7379I^{1/2})} \end{aligned} \quad (34)$$

Experimentally measured pH values are compared in Figure 4 with the predictions using the original K_{ca} expression from Oddo and Tomson,⁷ as shown in eq 15 and the modified K_{ca} equation (eq 34) at different temperatures. For all the

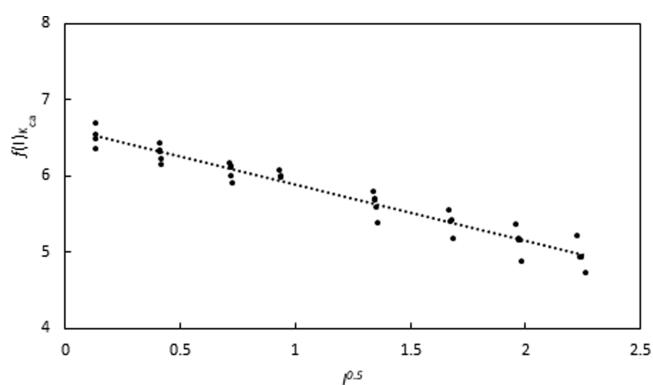


Figure 3. $f(I)_{K_{ca}}$ vs $I^{0.5}$ at different temperatures.^{12,36,37}

temperatures tested, from 5 to 80 °C (with a partial pressure of CO₂ ranging from 0.53 to 0.99 bar), the predictions using the updated K_{ca} expression not only exhibit the same trend as observed from measurements but also agree much better

(within 4% difference) with experimental values than Oddo and Tomson's equation. The improvement is especially significant in the more concentrated solutions (NaCl > 5 wt %).

Revision of $K_{sp,FeCO_3}$. In a manner similar to that for K_{ca} , the expression developed for $K_{sp,FeCO_3}$ is also recalibrated to better account for nonideality, for the presence of FeCl⁺ complex formation,²⁵ and for the change in the value of K_{ca} in CO₂ corrosion environments. $K_{sp,FeCO_3}$ represents the equilibrium state between precipitation and dissolution of FeCO₃. Under this circumstance, the value of $K_{sp,FeCO_3}$, as explained in eq 12, is expressed as the concentration product of freely available Fe²⁺_(aq) and CO₃²⁻_(aq). This means that at equilibrium $K_{sp,FeCO_3}$ can be directly calculated if $c_{Fe^{2+}}$ and $c_{CO_3^{2-}}$ are both known. Gao¹² calculated $K_{sp,FeCO_3}$ in this manner but failed to consider the FeCl⁺ formation and, consequently, $c_{Fe^{2+}}$ was overestimated. To correct this issue, the actual $c_{Fe^{2+}}$ in Gao's

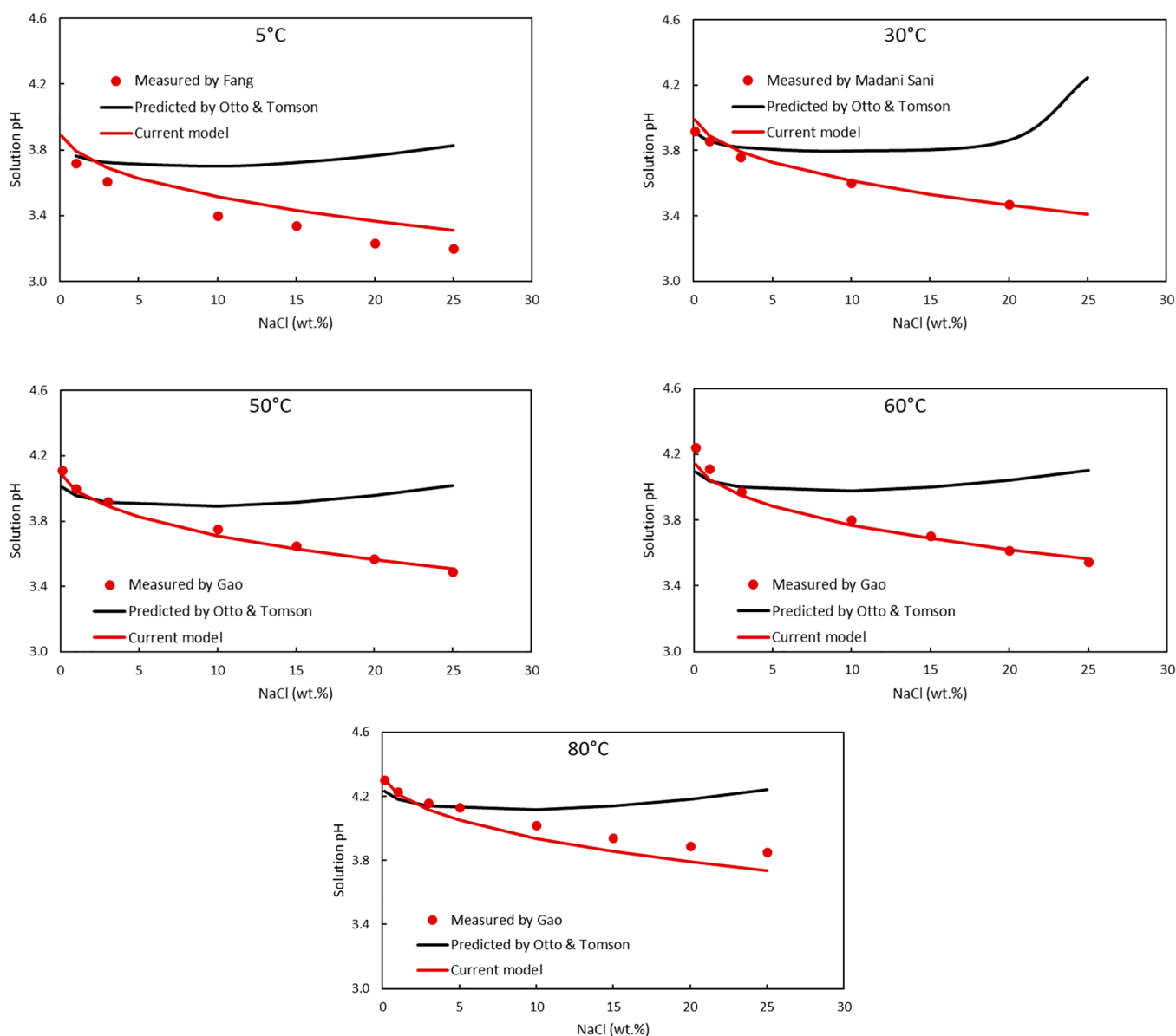


Figure 4. pH comparison between model calculations⁷ and experimental results^{12,36,37} at different temperatures.

work was recalculated using eq 24. In addition, the corresponding $c_{\text{CO}_3^{2-}}$ was also recalculated using the modified K_{ca} presented earlier (eq 34).

The correlation between $K_{\text{sp,FeCO}_3}$ and ionic strength can be explored using a similar methodology that has been used to extract K_2 and K_{ca} . The original expression for $K_{\text{sp,FeCO}_3}$ (eq 17) is rewritten to isolate the temperature- and ionic-strength-dependent terms (denoted as $f(I)_{K_{\text{sp,FeCO}_3}}$ in eq 35). An expression for $f(I)_{K_{\text{sp,FeCO}_3}}$ can easily be obtained by plotting the $f(I)_{K_{\text{sp,FeCO}_3}}$ against $I^{0.5}$.

$$\log K_{\text{sp,FeCO}_3} = f(I)_{K_{\text{sp,FeCO}_3}} - 0.041377T_{\text{K}} - \frac{2.1963}{T_{\text{K}}} + 24.5724 \log T_{\text{K}} \quad (35)$$

$$f(I)_{K_{\text{sp,FeCO}_3}} = \log K_{\text{sp,FeCO}_3} + 0.041377T_{\text{K}} + \frac{2.1963}{T_{\text{K}}} - 24.5724 \log T_{\text{K}} \quad (36)$$

As mentioned earlier, the experimental data used to perform the calibration are taken from Gao's work.¹² The experiments were conducted with brines containing salt concentration ranges from 1 to 25 wt % at 80 °C. The calculated $f(I)_{K_{\text{sp,FeCO}_3}}$ versus $I^{0.5}$ based on the above-mentioned procedure is presented in Figure 5, where the black dots are the calculations

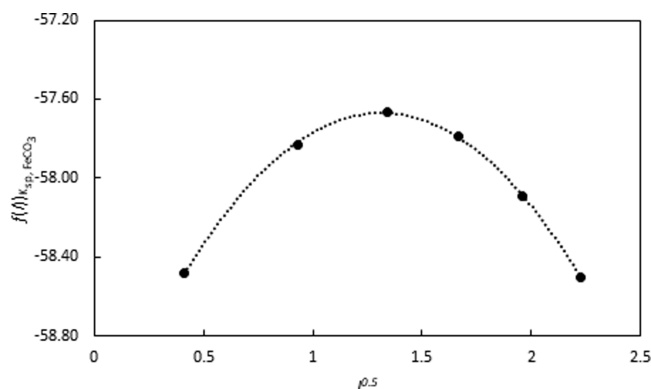


Figure 5. Fitting line for $f(\log K_{\text{sp,FeCO}_3})_{T_{\text{K}}}$ vs $I^{0.5}$ obtained at 80 °C.¹²

over six different salt concentrations. A modified expression of $K_{\text{sp,FeCO}_3}$ can now be determined from the best fit line, and its final equation is written in eq 37:

$$\log K_{\text{sp,FeCO}_3} = -59.4 - 0.041377T_{\text{K}} - \frac{2.1963}{T_{\text{K}}} + 24.5724 \log T_{\text{K}} + 2.6349I^{0.5} - 1.0027I \quad (37)$$

S_{FeCO_3} in Gao's work¹² are recalculated using the modified K_{ca} and $K_{\text{sp,FeCO}_3}$ expressions and plotted (diamonds) in Figure 6. The results are compared with the predicted S_{FeCO_3} (dots), calculated via Oddo–Tomson's K_{ca} ⁷ and the S&N model's $K_{\text{sp,FeCO}_3}$.²¹ The mass change due to FeCO_3 precipitation/dissolution is also included as a black line for ease of illustration. According to Gao, the measurement started in a FeCO_3 saturated solution with 1 wt % NaCl, and the author adjusted the solution pH to push the saturation of FeCO_3 to

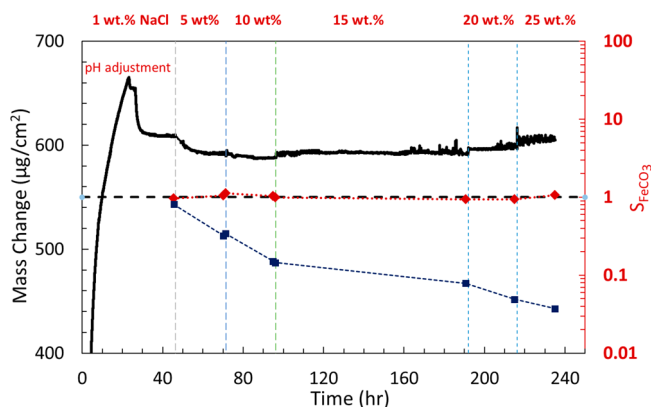


Figure 6. Mass change (black curve) of FeCO_3 precipitation and the corresponding S_{FeCO_3} calculated based on Oddo–Tomson's K_{ca} ⁷ and S&N model's $K_{\text{sp,FeCO}_3}$ ²¹ (navy blue dots) and that calculated based on modified K_{ca} and $K_{\text{sp,FeCO}_3}$ (red diamonds). Experimental values are taken from Gao's work at 80 °C, NaCl concentration 1–25 wt %.¹²

reach equilibrium ($S_{\text{FeCO}_3} = 1$). Additional NaCl was introduced into the solution in a stepwise manner (vertical dashed lines in Figure 6) to change the ionic strength of the solution. The mass change curve in the Figure 6 shows that the system always reached equilibrium (no significant mass change was observed over time) before further NaCl was added, so the S_{FeCO_3} at these points should be close to 1. The predicted S_{FeCO_3} based on the modified K_{ca} and $K_{\text{sp,FeCO}_3}$ coincide well, as expected, with all the data points (red diamonds), staying close to the line of $S_{\text{FeCO}_3} = 1$. The predicted S_{FeCO_3} (navy blue dots) calculated from Oddo–Tomson's K_{ca} ⁷ and S&N model's $K_{\text{sp,FeCO}_3}$,²¹ however, largely underestimated the saturation levels of the solution, especially when the solution contained high NaCl concentration. On the basis of these values, FeCO_3 should have continued dissolving, since the predicted S_{FeCO_3} values are well below 1. This is contrary to what was observed experimentally, since the system always reached equilibrium shortly after the injection of NaCl, showing no mass change (i.e., the FeCO_3 precipitation and dissolution rates were equal).

INVESTIGATION OF PRECIPITATION KINETICS OF FeCO_3 BY EQCM

As discussed, the model proposed by Ma et al.²⁴ was calibrated using the experimental data obtained in a 1 wt % NaCl electrolyte. The effect of solution salinity on FeCO_3 precipitation kinetics remains unclear and is explored here in solutions containing different dissolved NaCl concentrations. A series of experiments are conducted using an EQCM to accurately measure the rate of FeCO_3 precipitation on an iron substrate. In addition, the modified K_{ca} and $K_{\text{sp,FeCO}_3}$ expressions together with the reduction of Fe^{2+} due to the formation of FeCl^+ complex are considered in this work to characterize the electrolyte speciation and S_{FeCO_3} .

Experimental Procedure. All the precipitation experiments were conducted using a 2 L, three-electrode glass cell as shown in Figure 7. A Stanford Research System manufactured EQCM device, QCM200, and a 5 MHz At-cut Fe-coated quartz crystal with a 1.37 cm² effective area were used in this study. The aqueous solution with a controlled NaCl

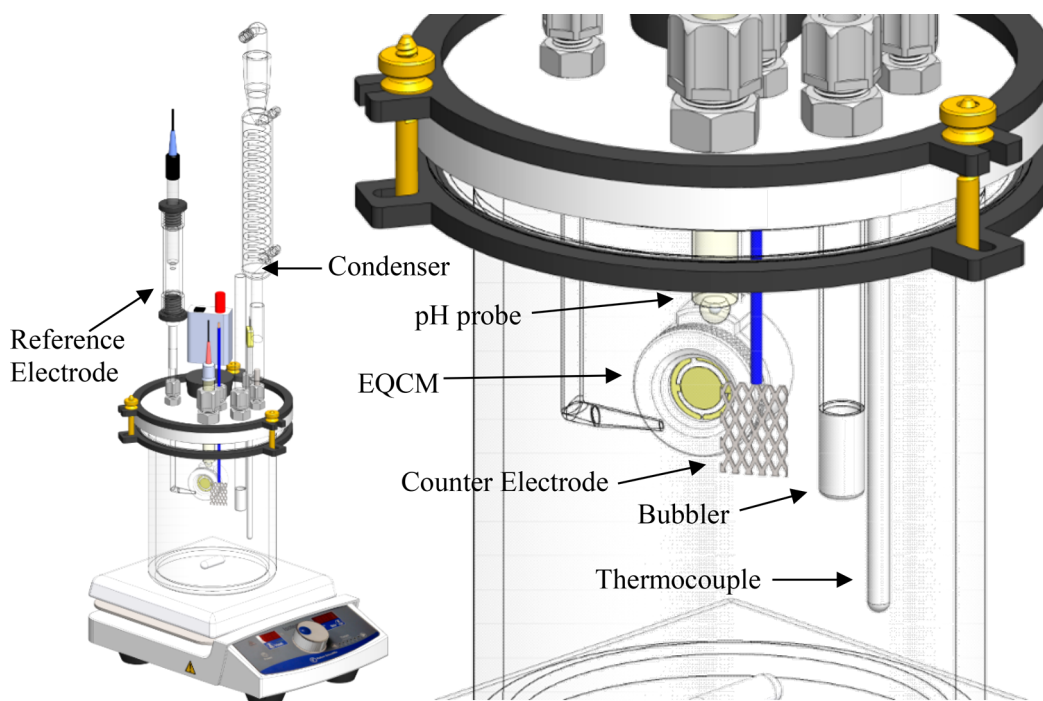


Figure 7. Experimental setup with EQCM (image printed with permission of Cody Shafer, ICMT).

concentration was deaerated by sparging with CO_2 gas for at least 2 h before starting the experiment, and the CO_2 sparging was maintained throughout the entire experiment to saturate the solution. The temperature of the solution was set to the desired value, and the solution pH was adjusted to 6.60 with deoxygenated NaHCO_3 solutions. The quartz crystal was installed into the EQCM holder and served as the working electrode. A platinum wire mesh was used as the reference electrode. A saturated silver–silver chloride (Ag/AgCl) electrode was used as the counter electrode. A potentiostat (Gamry Reference 600) was used to apply a specific potential as needed. A controlled volume of deaerated ferrous chloride ($\text{FeCl}_2 \cdot 4\text{H}_2\text{O}$) solution was added to provide additional Fe^{2+} and adjust the level of FeCO_3 saturation. During the measurement, bulk pH of the solution was recorded and $c_{\text{Fe}^{2+}}$ was measured by Genesis 10S Vis Spectrophotometer periodically. S_{FeCO_3} of the solution was calculated based on known solution pH, temperature, the pressure of CO_2 , and $c_{\text{Fe}^{2+}}$ according to eq 19. The methodology of measuring FeCO_3 precipitation rate using EQCM was explained in full detail by Ma et al.,²⁴ and the exact same approach was followed in this work. It is understood that FeCO_3 precipitation includes both the nucleation period and crystal growth period. The current work focuses on the growth period only. A summary of the experiment conditions is shown in Table 2.

Experimental Results and Discussion. Ma et al.²⁴ developed their latest model based on the measurement results obtained following the exact same experimental methodology; however, the work was done only at 1 wt % NaCl solutions.²⁴ It is consequently worth assessing whether the model (eq 18 with $k_{\text{r,FeCO}_3}$ ($3.32 \times 10^7 \text{ m}^4 \cdot \text{mol}^{-1} \cdot \text{s}^{-1}$) and $\Delta^*G_{\text{FeCO}_3}$ ($73\,739 \text{ J} \cdot \text{mol}^{-1}$)) can accurately predict the precipitation rate of FeCO_3 in more concentrated NaCl solutions.

Table 2. Experimental Matrix of FeCO_3 Precipitation in Solutions with Varied NaCl Concentrations

description	parameters
solution	3, 5, and 9 wt % NaCl
total pressure/bar	1
sparge gas	CO_2
initial solution pH	6.60 ± 0.05
stir bar speed/rpm	50
materials	polished Fe-coated quartz crystal
polarization	-0.05 to -0.1 V vs OCP
temperature/ $^\circ\text{C}$	60, 70, 80
initial $[\text{Fe}^{2+}]$ /ppm (wt)	~ 125

Figure 8 shows the measured $\text{PR}_{\text{FeCO}_3}$ in aqueous solutions with progressively higher NaCl concentration and the comparison with model predictions (shown as lines in the figure) using $\Delta^*G_{\text{FeCO}_3} = 73\,739 \text{ J} \cdot \text{mol}^{-1}$ and $k_{\text{r,FeCO}_3} = 3.32 \times$

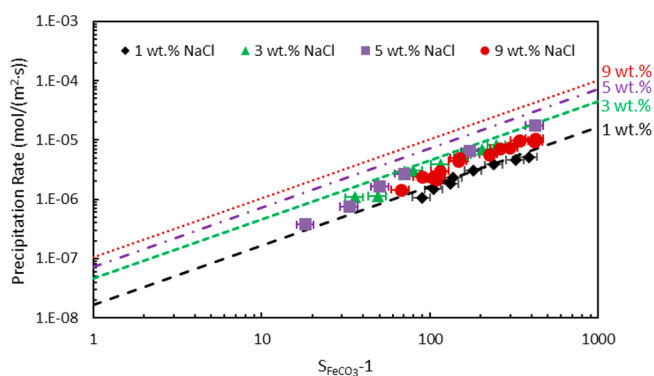


Figure 8. Comparison between model predictions and measured results in solutions with different NaCl concentrations at 80 °C, initial pH 6.60, and 0.53 bar CO_2 .

$10^7 \text{ m}^4 \cdot \text{mol}^{-1} \cdot \text{s}^{-1}$. The measured results in 1 wt % NaCl solution was obtained from Ma et al.,²⁴ and the S_{FeCO_3} was recalculated considering all the updates regarding K_{ca} , $K_{\text{sp,FeCO}_3}$, and the reduction of $c_{\text{Fe}^{2+}}$ (i.e., $c_{\text{Fe}^{2+ \text{ free}}}$ was used) as discussed in the previous section. It is clear that by using values for $k_{\text{r,FeCO}_3}$ and $\Delta^*G_{\text{FeCO}_3}$ extracted in 1 wt % NaCl solution the $\text{PR}_{\text{FeCO}_3}$ predicted from eq 18 agreed well with the EQCM measurements in 1 wt % NaCl solutions. However, the model does not provide accurate predictions when compared with measured results in more concentrated solutions: The predicted $\text{PR}_{\text{FeCO}_3}$ increases with the increase of NaCl concentration, while the measured values are closer together. No clear trend of $\text{PR}_{\text{FeCO}_3}$ can be extracted with respect to NaCl. This suggests that the values of these two kinetic related parameters need to be re-evaluated considering different solution ionic strengths to extend the validity of use. In addition, an approximately linear relationship between precipitation rate and S_{FeCO_3} still applies in NaCl concentrated solutions.

The $\text{PR}_{\text{FeCO}_3}$ values in NaCl concentrated solutions were also measured at 60 and 70 °C. Similar to what is shown in Figure 8, the predicted $\text{PR}_{\text{FeCO}_3}$ show a clear dependency on NaCl concentrations such that adding NaCl in solutions makes the precipitation of FeCO_3 faster, yet the measured $\text{PR}_{\text{FeCO}_3}$ values exhibit no clear correlation with NaCl concentration. A deviation between the predicted values and measured values exists, and this becomes more obvious in solutions with higher NaCl content. This is not surprising given that the $k_{\text{r,FeCO}_3}$ and $\Delta^*G_{\text{FeCO}_3}$ used here were taken from a solution with a relatively low NaCl concentration.

Updates in Activation Energy and Kinetic Constant in the FeCO_3 Precipitation Rate Equation. The previous section has shown that the model proposed by Ma et al.²⁴ fails in NaCl concentrated conditions due to the inaccurate activation energy and kinetic constant values. Updated values for the $\Delta^*G_{\text{FeCO}_3}$ and $k_{\text{r,FeCO}_3}$ are extracted based on experimental results. All the measured data are taken from previously presented FeCO_3 precipitation experimental results.

By taking a natural logarithm of both sides of the precipitation rate equation (eq 18), eq 38 can be obtained:

$$\ln \frac{\text{PR}_{\text{FeCO}_3}}{K_{\text{sp,FeCO}_3}(S_{\text{FeCO}_3} - 1)} = -\frac{\Delta^*G_{\text{FeCO}_3}}{RT} \ln k_{\text{r,FeCO}_3} \quad (38)$$

Therefore, if $\ln \frac{\text{PR}_{\text{FeCO}_3}}{K_{\text{sp,FeCO}_3}(S_{\text{FeCO}_3} - 1)}$ vs $\left(-\frac{1}{RT}\right)$ is plotted, then a straight line should theoretically be obtained with the slope being equal to the activation energy $\Delta^*G_{\text{FeCO}_3}$ and the y intercept being the $\ln k_{\text{r}}$ as shown in Figure 9, by taking 1 wt % experimental data as an example. The best fit line yielded $\Delta^*G_{\text{FeCO}_3} = 74\,398 \text{ J} \cdot \text{mol}^{-1}$ and $k_{\text{r}} = 4.99 \times 10^7 \text{ m}^4 \cdot \text{mol}^{-1} \cdot \text{s}^{-1}$ by using the average experimental value at each temperature.

The exact same methodology was followed to extract the two kinetics parameters in each different NaCl concentrated solutions. The corresponding values of these two parameters derived from all four measured conditions are summarized in Table 3. Notice that the NaCl concentration affected $\Delta^*G_{\text{FeCO}_3}$ and $k_{\text{r,FeCO}_3}$ in different ways. For $\Delta^*G_{\text{FeCO}_3}$, the changes of adding NaCl were minor enough that the deviation of

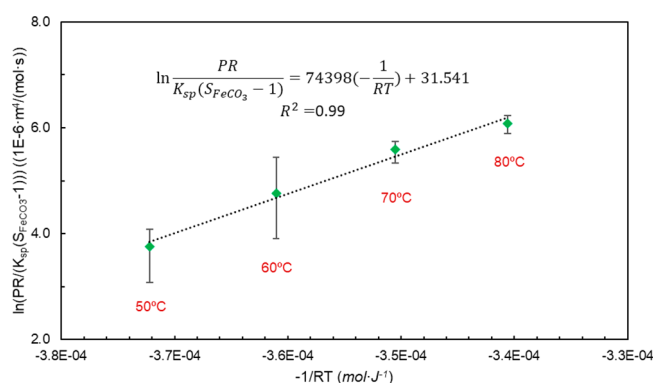


Figure 9. Best fit line for activation energy and kinetic constant in the FeCO_3 precipitation rate equation.

Table 3. Extracted $\Delta^*G_{\text{FeCO}_3}$ and $k_{\text{r,FeCO}_3}$ in Nonideal Solutions

wt % NaCl	ionic strength ($\text{mol} \cdot \text{L}^{-1}$)	$\Delta^*G_{\text{FeCO}_3}$ ($\text{kJ} \cdot \text{mol}^{-1}$)	$k_{\text{r,FeCO}_3}$ ($\text{m}^4 \cdot \text{mol}^{-1} \cdot \text{s}^{-1}$)
1	0.17	74.4	4.99×10^7
3	0.52	75.9	5.79×10^7
5	0.86	73.0	1.26×10^7
9	1.67	71.9	5.16×10^6

$\Delta^*G_{\text{FeCO}_3}$ was within 6%, whereas $k_{\text{r,FeCO}_3}$ changed by about 10-fold when the NaCl concentration increased from 1 to 9 wt %. This leads to the development of a new precipitation rate equation for FeCO_3 . It follows the same format as eq 18, yet the effect of NaCl concentration on both $\Delta^*G_{\text{FeCO}_3}$ and $k_{\text{r,FeCO}_3}$ are now considered:

$$\text{PR}_{\text{FeCO}_3} = (8 \times 10^7 e^{-1.7I}) \exp\left(-\frac{73800}{RT}\right) K_{\text{sp,FeCO}_3} (S_{\text{FeCO}_3} - 1) \quad (39)$$

in which $\Delta^*G_{\text{FeCO}_3} = 73\,800 \text{ J} \cdot \text{mol}^{-1}$ is the averaged value of $\Delta^*G_{\text{FeCO}_3}$ as listed in Table 3 and $k_{\text{r,FeCO}_3} = 8 \times 10^7 e^{-1.7I} \text{ m}^4 \cdot \text{mol}^{-1} \cdot \text{s}^{-1}$ with ionic strength, I , included in the exponent term (highlighted in red) was determined via the best fit line as illustrated in Figure 10.

The parity plots that compare the experimental and calculated FeCO_3 precipitation rates are shown in Figure 11. The graph on the left shows the predicted precipitation rate

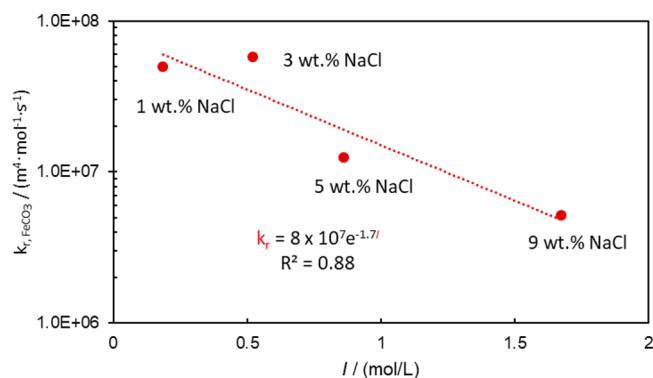


Figure 10. Extracted kinetic constant vs ionic strength on a semi-logarithmic scale.

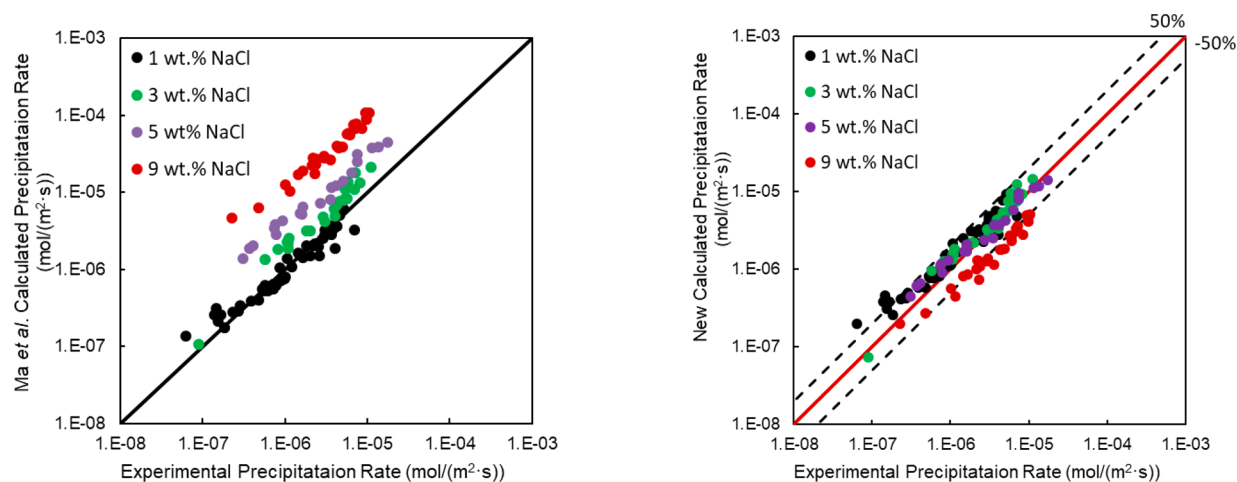


Figure 11. Parity plot showing comparisons between experimental and calculated precipitation using the outdated model proposed by Ma et al.²⁴ (left) and using the improved model, which includes all the updates discussed in this work (right).

using the equation proposed by Ma et al.²⁴ where $\Delta^*G_{\text{FeCO}_3}$ and k_{r,FeCO_3} are constants and based on 1 wt % NaCl solution. The graph on the right shows the predictions of the current model with the new correlations, which included all the improvements discussed in this paper. Most of the points on the left are above the diagonal line, meaning that the predictions are higher than the measurements, as illustrated in Figure 8, whereas the points on the right side of the plot are distributed closer together and much more evenly around the diagonal line, suggesting a significant improvement of fit. Most of the predicted precipitation rates with the new constants agree with the experimental values within a 50% difference.

CONCLUSIONS

Several modeling improvements impacting the accuracy of FeCO_3 precipitation kinetic calculations have been described: (i) The formation of FeCl^+ in the presence of NaCl significantly affects the actual free Fe^{2+} concentration and S_{FeCO_3} value. An ionic-strength-based equilibrium constant, K_2 , has been derived to estimate the dissociation degree of FeCl^+ . (ii) The dependency of K_{ca} on ionic strength has been re-examined. Rather than the quadratic correlation with $I^{0.5}$, as suggested by literature,^{7,12} $\log K_{\text{ca}}$ changes linearly with $I^{0.5}$. (iii) The expression of $K_{\text{sp,FeCO}_3}$ has been modified to include the effect of FeCl^+ complex formation and the updated K_{ca} expression. Using newly obtained experimental measurements, its dependency on ionic strength was also re-evaluated as the previously derived expression²¹ was found to considerably underestimate the actual S_{FeCO_3} value.

In addition, the precipitation rate of FeCO_3 was measured in solutions with varied concentration of NaCl within the temperature range 60–80 °C: (i) By using the values of k_{r,FeCO_3} and $\Delta^*G_{\text{FeCO}_3}$ calibrated from 1 wt % NaCl solution, the predicted value of $\text{PR}_{\text{FeCO}_3}$ using the Ma et al.²⁴ model agreed well with the EQCM measurements in 1 wt % NaCl solutions. However, this model tends to overestimate the FeCO_3 precipitation rate in NaCl concentrated solutions. (ii) Experimental $\text{PR}_{\text{FeCO}_3}$ measured via EQCM suggested that increasing NaCl from 1 to 9 wt % did not significantly change $\text{PR}_{\text{FeCO}_3}$. (iii) A kinetic model of FeCO_3 precipitation

considering the effect of nonideality was proposed. A significant improvement in $\text{PR}_{\text{FeCO}_3}$ prediction was obtained when comparing with the Ma et al.'s model.²⁴

It should be mentioned that all of the expressions derived in the current work are for use with NaCl. Caution should be used if different salts are present, especially for salts with divalent ions, as the ionic strength approach is an “engineering” approach that aims to express nonideality in a simplified way. For more robust predictions, an approach based solely on species activities, as introduced in eqs 21 and 24, should be followed.

AUTHOR INFORMATION

Corresponding Author

Marc Singer – Institute for Corrosion and Multiphase Technology, Ohio University, Athens, Ohio 45701, United States; orcid.org/0000-0002-0762-9755; Email: singer@ohio.edu

Authors

Zheng Ma – Institute for Corrosion and Multiphase Technology, Ohio University, Athens, Ohio 45701, United States
 Xin Gao – Institute for Corrosion and Multiphase Technology, Ohio University, Athens, Ohio 45701, United States
 Bruce Brown – Institute for Corrosion and Multiphase Technology, Ohio University, Athens, Ohio 45701, United States
 Srdjan Nescic – Institute for Corrosion and Multiphase Technology, Ohio University, Athens, Ohio 45701, United States

Complete contact information is available at: <https://pubs.acs.org/10.1021/acs.iecr.1c02957>

Notes

The authors declare no competing financial interest.

ACKNOWLEDGMENTS

The authors thank the following companies for their financial support: Ansys, Baker Hughes, BP America, Chevron Energy Technology, Clariant Corporation, CNOOC, ConocoPhillips, ExxonMobil, M-I SWACO (Schlumberger), Multi-Chem (Halliburton), Occidental Oil Company, Pertamina, Saudi

Aramco, Shell Global Solutions, Sinclair Energy Partners, SINOPEC (China Petroleum), and TOTAL.

REFERENCES

- (1) Nescic, S.; Sun, W. Corrosion in acid gas solutions. In *Shreir's Corrosion*, Cottis, B.; Graham, M.; Lindsay, R.; Lyon, S.; Richardson, T.; Scantlebury, D.; Stott, H., Eds. Elsevier: Oxford, 2010; pp 1270–1298.
- (2) Tran, T.; Brown, B.; Nescic, S. In *Corrosion of Mild Steel in an Aqueous CO₂ Environment – Basic Electrochemical Mechanisms Revisited*, CORROSION 2015, Dallas, Texas, Dallas, Texas, 2015.
- (3) Harvie, C. E.; Møller, N.; Weare, J. H. The prediction of mineral solubilities in natural waters: The Na-K-Mg-Ca-H-Cl-SO₄-OH-HCO₃-CO₃-CO₂-H₂O system to high ionic strengths at 25°C. *Geochim. Cosmochim. Acta* **1984**, *48* (4), 723–751.
- (4) Duan, Z.; Sun, R. An improved model calculating CO₂ solubility in pure water and aqueous NaCl solutions from 273 to 533 K and from 0 to 2000 bar. *Chem. Geol.* **2003**, *193*, 257–271.
- (5) Li, D.; Duan, Z. The speciation equilibrium coupling with phase equilibrium in the H₂O–CO₂–NaCl system from 0 to 250 °C, from 0 to 1000 bar, and from 0 to 5 molality of NaCl. *Chem. Geol.* **2007**, *244* (3), 730–751.
- (6) Zhao, H.; Fedkin, M. V.; Dilmore, R. M.; Lvov, S. N. Carbon dioxide solubility in aqueous solutions of sodium chloride at geological conditions: Experimental results at 323.15, 373.15, and 423.15 K and 150 bar and modeling up to 573.15 K and 2000 bar. *Geochim. Cosmochim. Acta* **2015**, *149*, 165–189.
- (7) Oddo, J. E.; Tomson, M. B. Simplified calculation of CaCO₃ saturation at high temperatures and pressures in brine solutions. *JPT, J. Pet. Technol.* **1982**, *34* (07), 1583–1590.
- (8) Palmer, D. A.; Van Eldik, R. The chemistry of metal carbonate and carbon dioxide complexes. *Chem. Rev.* **1983**, *83*, 651–731.
- (9) Zheng, Y.; Ning, J.; Brown, B.; Nescic, S. Advancement in predictive modeling of mild steel corrosion in CO₂- and H₂S-containing environments. *Corrosion* **2016**, *72* (5), 679–691.
- (10) Zheng, Y.; Ning, J.; Brown, B.; Nescic, S. Electrochemical model of mild steel corrosion in a mixed H₂S/CO₂ aqueous environment in the absence of protective corrosion product layers. *Corrosion* **2015**, *71*, 316–325.
- (11) Nordsveen, M.; Nescic, S.; Nyborg, R.; Stangeland, A. A mechanistic model for carbon dioxide corrosion of mild steel in the presence of protective iron carbonate films part 1: Theory and verification. *Corrosion* **2003**, *59* (5), 443–456.
- (12) Gao, X. Localized Corrosion Initiation of Steel in CO₂ Environment. Ph.D. Dissertation, Ohio University, Athens, OH, 2020.
- (13) Markham, A. E.; Kobe, K. A. The solubility of carbon dioxide and nitrous oxide in aqueous salt solutions. *J. Am. Chem. Soc.* **1941**, *63* (2), 449–454.
- (14) Greenberg, J.; Tomson, M. Precipitation and dissolution kinetics and equilibria of aqueous ferrous carbonate vs. temperature. *Appl. Geochem.* **1992**, *7* (2), 185–190.
- (15) Braun, R. D. Solubility of iron(II) carbonate at temperatures between 30 and 80°. *Talanta* **1991**, *38* (2), 205–211.
- (16) Marion, G. M.; Catling, D. C.; Kargel, J. S. Modeling aqueous ferrous iron chemistry at low temperatures with application to Mars. *Geochim. Cosmochim. Acta* **2003**, *67* (22), 4251–4266.
- (17) Helgeson, H. C. Thermodynamics of hydrothermal systems at elevated temperatures and pressures. *Am. J. Sci.* **1969**, *267* (7), 729.
- (18) Preis, W.; Gamsjäger, H. Critical evaluation of solubility data: enthalpy of formation of siderite. *Phys. Chem. Chem. Phys.* **2002**, *4* (16), 4014–4019.
- (19) Hogfeldt, E. *Stability Constants of Metal-Ion Complexes, Part A: Inorganic Ligands*; IUPAC Chemical Data Series; Pergamon Press, 1982.
- (20) Silva, C. A. R.; Liu, X.; Millero, F. J. Solubility of siderite (FeCO₃) in NaCl solutions. *J. Solution Chem.* **2002**, *31* (2), 97–108.
- (21) Sun, W.; Nescic, S.; Woollam, R. C. The effect of temperature and ionic strength on iron carbonate (FeCO₃) solubility limit. *Corros. Sci.* **2009**, *51* (6), 1273–1276.
- (22) Ma, Z.; Brown, B.; Nescic, S.; Singer, M. In Calculation of Surface Speciation on Mild Steel under Applied Polarization. Presented at CORROSION 2021, April 19, 2021; paper no. NACE-2021-16913
- (23) Sun, W.; Nescic, S. Kinetics of corrosion layer formation: part 1—iron carbonate layers in carbon dioxide corrosion. *Corrosion* **2008**, *64* (4), 334–346.
- (24) Ma, Z.; Yang, Y.; Brown, B.; Nescic, S.; Singer, M. Investigation of precipitation kinetics of FeCO₃ by EQCM. *Corros. Sci.* **2018**, *141* (15), 195–202.
- (25) Palmer, D. A.; Hyde, K. E. An experimental determination of ferrous chloride and acetate complexation in aqueous solutions to 300°C. *Geochim. Cosmochim. Acta* **1993**, *57*, 1393–1408.
- (26) Heinrich, C. A.; Seward, T. M. A spectrophotometric study of aqueous iron (II) chloride complexing from 25 to 200°C. *Geochim. Cosmochim. Acta* **1990**, *54* (8), 2207–2221.
- (27) Tomson, M. B.; Oddo, J. E. The Prediction of Scale and CO₂ Corrosion in Oil Field Systems. Presented at CORROSION 1999, San Antonio, TX, Jan. 1, 1999; NACE International: San Antonio, TX, 1999; p 16.
- (28) Dunlop, A. K.; Hassell, H. L.; Rhodes, P. R. Fundamental Considerations in Sweet Gas Well Corrosion. Presented at CORROSION 1983, Anaheim, CA; NACE International, 1983.
- (29) Dugstad, A.; Lunde, L.; Videm, K. Parametric Study of CO₂ Corrosion of Carbon Steel. Presented at CORROSION 1994, Baltimore, MD; NACE International, 1994.
- (30) van Hunnik, E. W. J.; Pots, B. F. M.; Hendriksen, E. L. J. A. In The Formation of Protective FeCO₃ Corrosion Product Layers In CO₂ Corrosion. Presented at CORROSION 1996, Houston, TX; NACE International, 1996.
- (31) Johnson, M. L.; Tomson, M. B. Ferrous Carbonate Precipitation Kinetics and Its Impact on CO₂ Corrosion, Presented at CORROSION 1991, Houston, TX; NACE International, 1991.
- (32) Helgeson, H. C.; Kirkham, D. H.; Flowers, G. C. Theoretical prediction of the thermodynamic behavior of aqueous electrolytes by high pressures and temperatures; IV, Calculation of activity coefficients, osmotic coefficients, and apparent molal and standard and relative partial molal properties to 600 degrees C and Skb. *Am. J. Sci.* **1981**, *281* (10), 1249–1516.
- (33) Pitzer, K. S. Thermodynamics of electrolytes. I. Theoretical basis and general equations. *J. Phys. Chem.* **1973**, *77* (2), 268–277.
- (34) WELLCORP is an equilibrium solver based on chemical potentials. Helgeson–Kirkham–Flowers equations of state (HKF EOS)³² are implemented to model the standard state chemical potential in electrolyte, and the Pitzer activity coefficient model³³ is implemented to model activity coefficients.
- (35) Batzle, M.; Wang, Z. Seismic properties of pore fluids. *Geophysics* **1992**, *57* (11), 1396–1408.
- (36) Madani Sani, F.; Brown, B.; Nescic, S. An electrochemical study of the effect of high salt concentration on uniform corrosion of carbon steel in aqueous CO₂ solutions. *J. Electrochem. Soc.* **2021**, *168* (5), No. 051501.
- (37) Fang, H. Low Temperature and High Salt Concentration Effects on General CO₂ Corrosion for Carbon Steel. Master of Science Thesis, Ohio University, Athens, OH, 2006.
- (38) Lyman, J. Buffer Mechanism of Sea Water. Ph.D. Thesis, University of California, Los Angeles, CA, 1956.
- (39) Mehrbach, C.; Culberson, C. H.; Hawley, J. E.; Pytkowicz, R. M. Measurement of the apparent dissociation constants of carbonic acid in seawater at atmospheric pressure. *Limnol. Oceanogr.* **1973**, *18* (6), 897–907.